DOI: 10.1002/ ((please add manuscript number))

Article type: Full Paper

Understanding the Orderliness of Atomic Arrangement towards Enhanced Sodium Storage

*Min Zhou, Yang Xu, Junxiang Xiang, Chengliang Wang, Liying Liang, Liaoyong Wen, Yaoguo Fang, Yan Mi, Yong Lei**

Dr. M. Zhou, Dr Y. X, Dr. C. W, L. Liang, Y. Fang, Dr. L. Wen, Y. Mi, Prof. Y. Lei

Institut für Physik & IMN MacroNano (ZIK)

Technische Universität Ilmenau, Ilmenau 98693, Germany

E-mail: yong.lei@tu-ilmenau.de

J. Xiang

Department of Materials Science and Engineering

University of Science and Technology of China, Hefei, 230026, P. R. China

Keywords: sodium-ion battery, orderliness, atomic arrangement, inverse opal, intercalation

In response to the increased demands of available energy storage, sodium ion batteries (SIBs) appear as promising alternatives to widely-used lithium ion batteries. However, because of large radius of Na ions, more complex requirements for the intrinsic properties raise the difficulties in finding a suitable material, in particularly for electrodes with intercalation mechanism. Concerning the principle of designing effective electrodes, the ordering of atomic arrangements should be at the heart in SIBs due to its significant influences on various electrochemical processes, such as ion absorption, ion diffusion, electron diffusion, *etc*. As proof-of-concept, the state-of-the art TiO_2 electrodes with different orderliness of atomic arrangement are achieved through colloidal crystal template method assisted by low-temperature atomic layer deposition and post-heating treatment. The disordering at the surface

is benefit for the faradaic contribution from surface processes, which is particularly significant to the electrode materials with poorer affinity of transporting ions. Meanwhile, the disordering in bulk results in better ion diffusion, but worse electrical transport. Understanding this relationship between atomic orderliness and battery performance is of importance for extending the design principle to some traditional electrodes for highly effective energy storage.

1. Introduction

Owing to the dependence on the consumption of fossil fuel, more and more serious environmental issues prompt a strong demand of green energy storage with high efficiency.[1] Among numerous available alternative technologies, secondary lithium-ion battery (LIB) has been regarded as predominant power source for electronics and vehicles now.[2] However, the scarcity of lithium, safety and cost form a potential obstacle for large-scale applications. Na, which is in the same series of alkali metal elements, possesses similar electrochemical properties with Li, but earth-abundance and low cost. So sodium-ion battery (SIB) becomes commercially competitive for with LIB.[3] Drawing inspiration from the similar rocking-chair mechanism with LIB, researchers has made rapid progress in identifying ideal electrodes, especially in the field of cathodes.[4] As for anodes, some state-of-the-art materials cannot accommodate the reversible intercalation of Na ions,[5] such as graphite.[6] The reasons mainly arise from the larger ionic radius of Na (1.02 Å) than Li (0.76 Å),[7] a higher ionization potential[8] and preferable coordination in octahedral or prismatic site of Na ions.[9] More complex requirements for the intrinsic properties raise the difficulties in finding a suitable material, in particularly for electrode with intercalation mechanism. A more open

framework is favorable for acceptable mobility, otherwise, the (de-)sodiation processes could induce large distortions in the lattice that ultimately lead to pulverization of the electrode and the impending failure of batteries.[10]

Concerning the discovery and design of ideal electrodes, the ordering of atomic arrangements is at the heart in SIBs, because the resulting changes on storage mechanism[11], surface state[12] and type/volume of polyhedral sites[13] play a vital role on the important electrochemical processes, like electrical conductivity, ion absorption, ion insertion, ion diffusion, and so on. Disordered atomic arrangements with isotropic characteristics may form percolation pathways *via* open some active diffusion channels to facilitate ionic transport, while long-range ordered atomic arrangements have the primary electro-active species of choice, and narrow potential window required to achieve the capacities.[14-15] With regard to SIB field, the controversy about the ordering seems obscure due to the large Na ions. Taking a typical electrode material, TiO_2, as an example, Xiong *et al.* proposed that long-range ordered polymorphs (*e.g.* anatase, rutile) cannot support Na-ion intercalation at all because of higher sodium diffusion barrier.[12] But Su *et al.* found anatase TiO_2 have superior capacities than disordered amorphous TiO_2.[16]

To reach a more accurate insight into the argument, a suitable platform is required for the systemic and scientific studies. Two factors of electrode design should be considered simultaneously. (1) The electrode should be tested without any conductive additive and polymeric binder, which will bring unclear changes on the electrical conductivity and surface state. (2) Morphological features of materials with different atomic ordering should be identical to avoid extra influences from surface area, electron/ion diffusion length, and so on. Therefore, it is highly desirable to explore a strategy that is capable of achieving TiO_2 architectures with precise structure and atomic ordering tuning. The architectures with

designed features must be stable during the tuning of the structural ordering. Inspired by above considerations and template confined method, we choose colloidal crystal templates[17, 18] and seek to realize the topological transformation from the templates using low-temperature atomic layer deposition (ALD) technique.[19] As shown in **Scheme 1**, the three-dimensional ordered porous architecture is constructed directly on the conductive substrate with identical morphologic features according to the templates, such as pore size, packing type of particles. Meanwhile, the operation at low temperature holds the promise to assure the integrity and the unique wall thickness in the architecture and the amorphous structural features with short-range ordered or disordered atomic arrangement. Subsequently, the ordering of atomic arrangements can be adjusted easily upon different heating treatment.

In this work, the state-of-the art electrodes in SIBs with different ordered degrees of atomic arrangement are achieved through colloidal crystal template method assisted by low-temperature ALD. Based on this platform, we correlate the battery performance with structural ordering. Different from previous reports in LIBs and NIBs, our results conclude that the disordering at the surface is benefit for the faradaic contribution from surface processes, which is particularly significant to the electrode materials with poorer affinity of transporting ions. But the more interrelations with electrolyte will decrease the long-term stability. Meanwhile, the disordering in bulk results in better ion diffusion, but worse electrical transport. Understanding this relationship between atomic ordering degree and battery performance is of importance for systematically adjusting and finally extending the design principle to some traditional electrodes for highly effective energy storage.

2. Results and Discussions

The actualization of this tentative architecture is revealed in **Figure 1a**.[20] Polystyrene spheres (PSs) are self-assembled to form colloidal crystal template directly on the conductive Ti foil. Then low-temperature atomic layer deposition (ALD) is employed as the infiltration technique to realize the complete topological transform from the templates. To ensure disordered nature and avoid the huge deformation above the PSs' glass transition (98 °C), we choose 70 °C as the deposition temperature after optimization, and then the as-prepared intermediate is immersed into Tetrahydrofuran (THF) for 48 h in ambient air to remove the template *via* dissolution. The featureless X-ray diffraction (XRD) pattern and Raman spectra of pristine sample in **Figure 1b** and **1c** (red) indicates disordered atomic arrangement. Post-heating process has been regarded as a facile and straightforward procedure to change the order degree of atomic arrangement. Upon annealing at different temperatures, it is clear seen from the XRD patterns in Figure 1b that the atoms becomes more ordered to form anatase TiO_2 (I41/amd) above 350 °C. As well known, XRD indicates the long-range order of materials and offers average structural information within several unit cells. Raman scattering as a local probe is more sensitive to local symmetry of materials.[21] The Raman modes of anatase TiO_2[22] appear at the spectra of samples after annealing at 350 °C, where no peaks can be observed from pristine sample without annealing. The comparison indicates the long-range orderliness of atomic arrangement. Furthermore, two characteristic peaks in X-ray photoelectron spectroscopy (XPS) (458.6 eV and 464.4 eV) manifests that Ti ions are mainly presented as Ti^{4+} in the lattice within all the samples instead of Ti^{3+} or Ti^0[23-24]. As for the pristine sample after annealing at 250 °C, it is worth noting that although there are no peaks belonged to anatase TiO_2 appearing in the XRD pattern, the obvious peak in Raman spectra proves that the atomic arrangement turn to be more ordered and forms partial symmetry. In this sense, the TiO_2 architectures with different order degrees of atomic arrangements are well realized to validate this rational design. Considering that anatase structure is the most feasible

matrix for the reversible intercalation of Na ions because of possible interstitial sites based on the stacking TiO_6 octahedraons and suitable paths for ion diffusion, we choose anatase as the reference with long-range order. For the purpose of visualized understanding, hereafter, as shown in Figure 1b-1d, the pristine sample without annealing is designated as sample with disordered (DO) atomic arrangement, whereas the samples after annealing at 350 °C are designated as samples with long-range ordered (LO) atomic arrangement. Similarly, we name the sample after annealing at 250 °C as partially ordered (PO) sample.

To further make sure the unique morphological features, we perform the observations from the scanning electron microscopic (SEM) images and transmission electron microscopic (TEM) images (**Figure 2**). The morphological features nearly keep the same upon different annealing temperatures. All the electron microscopic images demonstrate similar inverse opal morphology with high degree of hexagonal symmetry, which is the completely transformed from colloidal crystal template using ~500 nm polystyrene spheres (PSs). More details seen from TEM images in **Figure 2c, 2h and 2m** confirm that the periodic packing of hollow spheres with unique diameter (~500 nm) and wall thickness (~20 nm) are connected with each other to make open channels that allow a continuous skeleton with a three-dimensionally interconnected pore system. Although LO, PO and DO share nearly all the same geometrical characteristics, when carefully observing the SEM images at high magnification, we find that the surface of LO is much rougher than that of DO and PO, in compliance with the TEM results. This variation could be ascribed to the increased degree of atomic order and correspond formation of anatase crystalline particles as evidenced from the high-resolution TEM images. No discernible lattice fringe can be observed in DO and PO (**Figure 2d, 2i**), while we could find clear lattice fringe in LO that are assigned to (010) facet in anatase TiO_2. These results are in accord with above-mentioned conclusions from XRD and Raman analysis,

together with the proofs from featureless selected area electron diffraction (SAED) pattern of DO (**Figure 2e, 2j**) and clear fast Fourier transform (FFT) images of LO (**Figure 2o**).

To quantify the activity towards Na-ion storage, two-electrode coin cells with TiO_2-based working electrode and Na disk counter electrode are employed as a half-cell configuration. Since the interconnected porous architectures are fabricated directly on the conductive substrate, it is not necessary to add any conductive additive and polymeric binder, which may introduce uncertain influences to hinder the observations between atomic and SIB performance. Cyclic voltammetry (CV) are first recorded to elucidate the redox processes in host matrix with different degree of atomic ordering. Shown in **Figure 3a** are the CV curves of the 10^{th} cycle at a sweep rate of 0.1 mV s^{-1} in the potential range of 0.01−3.0 V (*vs.* Na/Na^+), where the curves of 1^{st} and 5^{th} cycles are illustrated in **Figure S1**. Regarding the CV curve of LO, a redox couple at 0.82 V (anodic) and 0.66 V (cathodic) indicates the reversible insertion/extraction of sodium.[25] In the case of DO and PO, no peaks appear over the entire potential range, indicating the wide distribution of redox events associated with broad energy dispersion of sodiation sites. Comparing with the three curves, we assert that differences in Faradaic processes of sodium storage can be fully ascribed to differences in degree of atomic order.

More information can be revealed from the voltage profiles to illustrate the electrochemistry of (de-)sodiation in the host. As shown in **Figure 3b-3d**, we list the discharge voltage profiles of 1^{st}, 2^{nd}, 20^{th} and 50^{th} cycles at 50 mA g^{-1}. Compared with the profiles among DO, PO and LO after different cycles, DO and PO exhibits a slop feature, while the plateau is more obvious in LO's curves. These appearances further evidence the CV analysis of redox. More noteworthy, the initial discharge capacity of DO is 408.9 mA h g^{-1}, while the value turns to 218.2 mA h g^{-1} after 50 cycles. In case of LO TiO_2, the specific capacities are 280.9 and 219.1

mA h g^{-1}. PO shows medium performance in both capacity and stability to bridge the electrochemical properties between DO and LO. These values represent the high specific capacity within various pure TiO_2 anodes as evidenced in Table S1[5, 10, 12, 15, 26] and even higher or comparable to composite TiO_2 systems,[25, 27-28] implying that both LO, PO and DO TiO_2 possess excellent ability of sodium storage.

To illuminate the effects of atomic ordering on sodium storage, the cycle stability at different charging/discharging current densities and rate performance of these half-cells are depicted in **Figure 4**. As a comparatively low current density, 50 mA g^{-1}, the specific capacities of SO and LO TiO_2 still remain 171 and 202.9 mA h g^{-1} even upon 200 cycles (**Figure 4a**). Both the values stand out among numerous TiO_2-based electrodes in SIBs because of the long-term stability.[5, 12, 16, 25] When carefully observing this segment, we find that DO possesses higher capacities at the initial several cycles, but suffers from a rapid fading of capacities. In other words, the stability of LO is comparatively better. The retention reaches 92.5 % from 50 cycles to 100 cycles. However, concerning the charging/discharging current density increasing to 500 and 2000 mA g^{-1} (**Figure 4b** and **4c**), all DO, PO and LO show the good stabilities, implying that high-rate Na-ion insertion/extraction into the hosts is feasible. A close look at the capacities at high rates suggests better sodium storage of DO than LO. The comparison of rate performance in **Figure 4d** and **S2** further confirms the evolution of the specific capacities upon cycling. Overall, since Ti foil as the substrate contributes little to the final capacity (**Figure S3**) and the morphology features keep unique, the striking differences in electrochemistry are completely attributed to the order degree of atomic arrangement. Analysis of the cycling and rate performance of disordered and long-range ordered TiO_2 allows us to draw the following conclusions: (1) All disordered, partially ordered and long-range ordered TiO_2 with periodic porous architectures are potential candidates for high

performance SIB because of superior rate capacities and cycling stability, in particularly at high rates. (2) Disordered TiO_2 shows better rate performance both in capacities and stability at high rates. (3) Long-range ordered TiO_2 exhibits excellent long-term stability at low rate. (4) Partially ordered TiO_2 possesses medium electrochemical performance between LO and DO. Hence, the degree of atomic order indeed plays a visible role on SIB performance.

In order to systemically understand why the degree of atomic order can influence the battery performance so much, an investigation of thermodynamics is helpful to gain insight to the feasibility and reversibility of the process. With regard to the sodium storage mechanism, according to the XRD patterns after long-term cycling in **Figure S4**, invisible peaks from Na_2O *etc* or other extra products indicate a reversible $Ti^{4+}/^{3+}$ redox and Na-ion intercalation mechanism, being consistent with studies in previous literatures.[28-29] The overall reaction can be written as

$$TiO_2 + xNa \leftrightarrow Na_xTiO_2$$

After simulation and structural optimization, the sodium storage in both disordered and long-range ordered TiO_2 is possible up to one Na per TiO_2 (*i.e.* x=1), yielding the theoretical capacity as high as 335 mAh/g. As shown in **Figure 5a** and **5b**, because of the large radius, Na ions prefer to occupy interstitial octahedral positions.[30] Fortunately, the volume of octahedral site in LO (anatase) is large enough for the accommodation. Meanwhile, disordered atomic arrangement in DO can create larger or smaller spatial sites than those in LO. So on average, the thermodynamic ability for (de-)sodiation is similar between SO and LO in theory.

However, what is the possible origin of the gaps between the SIB performance of DO and LO? With the understanding in thermodynamics established, we turn our eyes on the kinetic factors. As well known, CV is a powerful approach to illuminate the electrochemical kinetics

of the electrodes towards Na ions. **Figure 6a, 6c** and **6e** display the CV curves of DO, PO and LO at various sweep rates from 0.1 to 5 mV s^{-1}. Regarding to the contributions to total sodium storage, there are two typical types[12]: (1) the faradaic contribution from Na-ion intercalation; (2) the surface faradaic pseudocapacity and nonfaradaic double-layer capacity. Generally, we can infer the contributions of different mechanisms through CV analysis with the help of varying rates: [28-29]

$$i = a\upsilon^b \quad (1)$$

Therefore, by plotting log(i) against log(υ), we can obtain b value from the slopes. In general, *b*-value should be 0.5 if the sodium storage is dominated by bulk diffusion, whereas the b-value of 1.0 represents a pure capacitive process. The detailed explanation can be found in supporting information. As depicted in Figure 5b, the b-values of LO are larger than 0.95 over the wide potential range, which is close to 1, indicating the surface pseudocapacitative mechanism. So does PO. As for LO, *b*-values are calculated based on the current at peak potential, because the diffusion process is most feasible at this region.[28] Surveying from **Figure 5d**, the *b*-values of 0.89 and 0.90 are quantified for anodic and cathodic peaks, respectively. So even current at peak potential are mainly generated from capacitance. Such results confirm that most sodium storage within DO, PO and LO comes from the surface storage instead of bulk redox reaction between Ti^{4+}/Ti^{3+}, which is different with the mechanism in LIBs.[18, 31]

Such an important result inspires us to first pay our attention on the detailed kinetic impacts from atomic arrangements at surface. When looking carefully into the cycling performance at 50 mA g^{-1}, it is easy to find that the specific capacities of DO and LO decrease along with cycles like most reported electrodes, however, when the charging/discharging current density increasing to 500 mA g^{-1}, LO undergoes a self-improving process with 42 cycles to achieve

the highest capacitance as shown in **Figure 4b** and **7a**, which tends to be prolonged with increased rates. If the current density further increases to 2000 mA g^{-1}, the self-improving process further extend to 160 cycles, whereas the capacities of DO suffers only 10-cycle self-improving. With regard to PO, the number of self-improving cycles is 41.

Several competing mechanisms might be used to explain the observed differences. Some studies conclude that the origin of the self-improving stage is attributed to the electrochemically driven phase transformation or continually formation of SEI layer due to the exfoiliation of active materials. Since the XRD patterns and SEM images after cycling (**Figure S4** and **S5**) prove the stable phase and overall integrity of complex porous architectures, so we can exclude possible influences from phase and morphology. Meanwhile, considering the self-improving process appears at the initial stage of cycles, more possibilities are attributed to the influences of surface kinetics. A survey of literatures illustrates that similar varying can also be observed at fast cycling in LIBs[12] because of insufficient Li-ion concentration to support fast cycling. In the case of SIBs, larger radius leads to poorer affinity of Na ions to TiO_2 surface. It was previously observed that Li ions adsorb strongly on the surface of TiO_2 in aprotic electrolyte solutions, whereas no adsorption of Na ions can be found under the same conditions.[32] So a relatively high concentration of Na ions need to first be established near the surface, then Na ions can concentrate at reduced Ti centers, and finally diffuse into the TiO_2 matrix. Insufficient ion availability near the surface can account for observed self-improvement of the capacities upon cycling at slow cycling. This understanding implies that disordered atomic arrangement in DO possesses a surface with higher potential for Na-ion absorption, leading to more effective surface ion availability than that of long-range ordered TiO_2 (LO). This view can be evidenced from the much lower absorption energy of Na ions in propylene carbonate (PC) at disordered surface of DO as shown in **Figure 7b**.

Considering the similar morphology parameters, we contribute this enhanced absorption to the roughness on atomic level, where more potential defects induced by disordered atomic arrangement, such as dangling bonds and vacancies, enables stronger attraction of Na ions.[33] Moreover, the poorly defined atomic arrangement with thermodynamically metastable energetic state as compared to crystalline surface generates more open channels with enough volume for better penetration of Na ions, while some unexpected electronic states are expected to raise electric conductivity near the surface.[34] So low order degree of atomic arrangement at surface is helpful to voluntarily maintain a sufficient ion concentration near the surface for supporting the fast cycling in short time. That's why DO have shorter self-improving cycles and better rate capacities. To prove this hypothesis, electrochemical impedance spectra (EIS) are conducted after different cycles (**Figure S6**). As shown in **Figure 7c**, DO and PO shows much lower charge transfer resistance (R_{ct}) than LO, and the gap becomes larger and larger with increased cycles. Since all the sodium storage are limited by the surface capacitive process, R_{ct} mainly depend on the charge transfer resistance related to the redox reaction across the electrode/electrolyte interface.[35] Smaller R_{ct} suggests much easier reactions at surface. Therefore, the disordering at the surface is indeed benefit for the faradaic contribution from surface processes, which contribute major capacities to the whole sodium storage.

Beside the surface reaction, bulk sodium storage is another important component. During this process, two vital kinetic factors should be considered: electron transport and ion diffusion. To obtain more insight into charge transport within the electrodes and the electrical contact at the current collector interface, we next check the resistance of DO, PO and LO. The resulting symmetrical and linear appearance of I-V curves in **Figure 8a** display the Ohmic contacts between the electrode and conductive substrate.[36] However, LO possesses smallest resistance

throughout the whole matrix. Facile electron transport could be realized in long-range ordered TiO_2 rather than in disordered TiO_2. With respect to ion diffusion, as shown in Figure 5b, Na ions are favorable to occupy the octahedral sites in long-range ordered anatase TiO_2. For the purpose of ion diffusion, all the Na ions hop between the neighboring octahedral sites. They are forced to travel along the shared octahedron edges because of the strong electrostatic repulsion between Na and adjacent Ti drives.[37] Two Na-O_6 octahedrons will suffer distinct distortion to allow Na-ion hop between them, and thus the shared edge of the two octahedrons changes between 3.56 and 4.02 Å,[38] which causes huge energy barrier upon Na-ion diffusion. According to the simulation, if one Na can completely insert into anatase TiO_2, the lattice will suffer 32.23 % expansion in volume ($NaTiO_2$ *vs.* TiO_2). However, disordered atomic arrangements offer a more open framework to facilitate ion transport and tolerance the distortion during (de-)sodiation. So the Na-ion diffusion is facilitated in disordered TiO_2 rather than long-range ordered TiO_2, which can be evidenced by the Na-ion diffusion coefficients (D_{Na+}) after cycles as depicted in **Figure 8b and S7**. The Na-ion diffusion in disordered TiO_2 is nearly 300-times than that in long-range ordered TiO_2. (6.56×10^{-10} cm^2 s^{-1} *vs.* 2.11×10^{-12} cm^2 s^{-1}). This variation may result from the difficult diffusion barrier of Na ions in long-range ordered matrix because of the requirements based on crystalline symmetry. More ratio of shortened Ti-O bond decreases mobility and increase the difficulties of diffusion in LO.

As electron diffusion coefficient are magnitudes higher than that of Na ions,[38] DO TiO_2 would only increase a smaller electron diffusion resistance but gain a large decrease of Na-ion diffusion resistance. Overall, the disordered atomic arrangement in bulk will prompt the faradaic contribution from Na-ion intercalation. So DO shows comparatively high capacities at different rates, especially at initial stage.

Given these analysis, our results prove that the disordering at the surface is benefit for the faradaic contribution from surface processes, in particularly significant to the electrode materials with poorer affinity of transporting ions. The disordering in bulk results in better ion diffusion, but worse electron transport. As mentioned above, the disordered atomic arrangement at surface provides a roughness surface at atomic level, which can improve the attraction to Na ions. However, some side reactions with electrolyte may also become easier. Following this rule, strategies to further enhance the electrochemical sodium storage of TiO_2 should concentrate on the surface reconstruction and electrolyte choice to promote the long-term stability and rate performance. Though the relative study is beyond our present work, we are looking forward to more effort in these open questions in the near future.

3. Conclusion

As proof-of-concept, inverse opal TiO_2 electrodes are realized with controllable orderliness of atomic arrangement. With the help of low-temperature atomic layer deposition technique, identical morphologic features and stability against the temperatures allow a suitable platform for observing the influences from orderliness of atomic arrangement on sodium storage. As proved by the good rate performance and cycling stability, inverse opals with both disordered and long-range ordered TiO_2 (anatase) are promising candidates for high performance SIBs. The different electrochemical behaviors are attributed to the intrinsic atomic arrangement. According to the he thermodynamics analysis, share similar ability for (de-)sodiation. However, the orderliness of atomic arrangement results in different kinetics barrieres in various electrodechemical processed. The disordering at the surface is beneficial for the faradaic contribution from surface processes, in particularly significant to the electrode materials with poorer affinity of transporting ions. The disordering in bulk results in better ion diffusion, but worse electron transport. The understanding of employing orderliness paradigm

into electrode design provides a powerful design foundation for realizing efficient energy storage. Further engineering of atomic ordering on traditional materials is expected to stimulate more research interests in the development of sodium-ion batteries.

4. Experimental Section

Assembly of Colloidal Crystal Templates. The well-ordered colloidal crystal templates were fabricated by polystyrene spheres (PSs) directly on the conductive Ti foils, which have been cleaned under sonication by sequentially acetone, ethanol and distilled water. Then Ti foils were immersed vertically in the 0.5 wt% polystyrene latex at 60 °C. The drying of sample at very low speed under large moisture can prevent the occurrence of cracking.

Fabrication of disordered, partially ordered and long-range ordered TiO_2 architectures. In a typical procedure, disordered TiO_2 were fabricated by low-temperature atomic layer deposition on the surface of the colloidal crystal templates using a PicoSun SUNALETM R-150 ALD system (PicoSun, Finland) according to the following procedure. The reaction temperature was set as 70 °C after optimization, and $TiCl_4$ and H_2O were chosen as the precursors. $TiCl_4$ was pulsed for 0.1 s and purged for 10 s, followed by a 0.1 s pulse and 10 s purge of H_2O. This procedure was repeated for 600 cycles. Then the as-prepared intermediate is immersed into Tetrahydrofuran (THF) for 48 h in ambient air to remove the template *via* dissolution. Partially ordered and long-range ordered samples followed the same processes, and then underwent a post-heating treatment at high temperatures, such as 250 and 350 °C for 2 h.

Characterization. X-ray diffraction (XRD) mearsurement was performed on a SIEMENS/BRUKER D5000 X-ray diffractometer using Cu-Kα radiation at 40 kV and 40 mA, with scanning range within $2\theta = 20°\text{-}80°$ at rate of $0.02° \ s^{-1}$ in a Bragg-Brentano geometry.

Raman spectra were recorded by an inVia Raman microscope with a 514.5 nm Ar laser. X-ray photoelectron spectroscopy (XPS) were carried out on a VG ESCALAB MK II X-ray photoelectron spectrometer with an exciting source of Mg Kα = 1253.6 eV. The binding energies were corrected for specimen charging by referencing C 1s to 284.5 eV. Scanning electron microscopy (SEM) analysis was performed on a Hitachi S4800 field emission scanning microscopy. Transmission electron microscopy (TEM) analysis and selected area electron diffraction (SAED) patterns were conducted by JEM-2010F (JEOL).

Electrochemical measurement. The as-prepared disordered and long-range ordered TiO2 architectures were directly used as anodes without adding any conductive additive and polymeric binder. Electrochemical mearsurements were performed through a coin cell configuration (CR2032) with a 20 mm diameter and 3.2 mm thickness. All the assembly processes were carried out in a nitrogen-filled glove box with oxygen and moisture concentrations kept below 0.1 ppm. Sodium metal disk used as a counter electrode was separated from the working electrode with the help of a glass microfiber filter (Whatman, Grade GF/B) (pore size: 1 μm). The electrolyte is 1 mol L^{-1} sodium perchlorate ($NaClO_4$) in propylene carbonate (PC, Aldrich anhydrous 99.7%). Cyclic voltammetry (CV) was recorded by a VSP electrochemical workstation (Bio-Logic, France) with different scan rates in the potential range of 0.01 to 3.0 V (*vs.* Na/Na^+). All these measurements were performed under ambient temperature (20 ± 2 °C). The mass loading of DO is around 0.42-0.45 mg, while that of LO is around 0.40-0.42 mg.

Simulation of atomic arrangements before and after Na intercalation. To create the disordered TiO_2 (DO-TiO_2) model, we compacted anatase-TiO_2 fragments into a cell fixing density of 4.23g cm^{-3} and total atoms of 48 O and 24 Ti. The Na inserted TiO_2 was formed by

adding Na into the TiO_2 interspace and the structure was relaxed several times using Dynamic Simulation method before further geometry optimization.

Simulation of Na-ion absorption energy. We calculated adsorption energy of anatase-TiO_2 ((0 0 1), (1 0 0), (0 1 0), and (1 1 0) surface) and TiO_2 with disordered atomic arrangement. In this calculation, the adsorption energy is defined as the energy change when adsorbing a single layer of Na^+ on the surface. All surface models used had 20 angstrom vacuum slab to prevent interaction between two periods. The most possible adsorption position was identified by Monte Carlo search using Adsorption Locator module in Materials Studio. Dmol3 was used to carry out geometry optimization and energy calculation. We used GGA-PBE as exchange-correlation potential, and solvent effect was included as well. Energy calculation was converged to $1x10^{-6}$ and geometry optimization convergence was set to $1x10^{-5}$.

Supporting Information

Supporting Information is available from the Wiley Online Library or from the author.

Acknowledgements

This work was supported by a European Research Council Grant (Three-D Surface: 240144) and Federal Ministry of Education and Research in Germany (BMBF: ZIK-3DNano-Device: 03Z1MN11;).

Received: ((will be filled in by the editorial staff))
Revised: ((will be filled in by the editorial staff))
Published online: ((will be filled in by the editorial staff))

[1] B. Dunn, H. Kamath, J.-M. Tarascon, *Science* **2011**, *334*, 928.

[2] B. Nykvist, M. Nilsson, *Nature Clim. Change* **2015**, *5*, 329.

[3] a) M. D. Slater, D. Kim, E. Lee, C. S. Johnson, *Adv. Funct. Mater.* **2013**, *23*, 947; b) N. Yabuuchi, K. Kubota, M. Dahbi, S. Komaba, *Chem. Rev.* **2014**, *114*, 11636; c) C. Wang, Y. Xu, Y. Fang, M. Zhou, L. Liang, S. Singh, H. Zhao, A. Schober, Y. Lei, J. Am. *Chem. Soc.* **2015**, *137*, 3124; d) L. P. Wang, L. Yu, X. Wang, M. Srinivasan, Z. J. Xu, *J. Mater. Chem. A* **2015**, *3*, 9353; e) K. Kubota, S. Komaba, *J. Electrochem. Soc*. **2015**, *162*, A2538.

[4] a) P. Barpanda, G. Oyama, S.-i. Nishimura, S.-C. Chung, A. Yamada, *Nat. Comm.* **2014**, 5; b) N. Yabuuchi, M. Kajiyama, J. Iwatate, H. Nishikawa, S. Hitomi, R. Okuyama, R. Usui, Y. Yamada, S. Komaba, *Nat. Mater*. **2012**, *11*, 512; c) G. Venkatesh, V. Pralong, O. I. Lebedev, V. Caignaert, P. Bazin, B. Raveau, *Electrochem. Comm.* **2014**, *40*, 100.

[5] L. Wu, D. Bresser, D. Buchholz, G. A. Giffin, C. R. Castro, A. Ochel, S. Passerini, *Adv. Energy Mater.* **2014**, *1401142*.

[6] D. A. Stevens, J. R. Dahn, *J. Electrochem. Soc.* **2000**, *147*, 4428.

[7] Y. Xu, M. Zhou, X. Wang, C. Wang, L. Liang, F. Grote, M. Wu, Y. Mi, Y. Lei, *Angew. Chem. Int. Ed.* **2015**, *54*, 8768.

[8] Y. Fang, L. Xiao, J. Qian, X. Ai, H. Yang, Y. Cao, *Nano Lett.* **2014**, *14*, 3539.

[9] J. Qian, X. Wu, Y. Cao, X. Ai, H. Yang, *Angew. Chem. Int. Ed*. **2013**, *52*, 4633.

[10] X. Yang, C. Wang, Y. Yang, Y. Zhang, X. Jia, J. Chen, X. Ji, *J. Mater. Chem. A* **2015**, *3*, 8800.

[11] H. Xiong, H. Yildirim, E. V. Shevchenko, V. B. Prakapenka, B. Koo, M. D. Slater, M. Balasubramanian, S. K. R. S. Sankaranarayanan, J. P. Greeley, S. Tepavcevic, N. M. Dimitrijevic, P. Podsiadlo, C. S. Johnson, T. Rajh, *J. Phys. Chem. C* **2012**, *116*, 3181.

[12] H. Xiong, M. D. Slater, M. Balasubramanian, C. S. Johnson, T. Rajh, *J. Phys. Chem. Lett*. **2011**, *2*, 2560.

[13] V. Mathew, S. Kim, J. Kang, J. Gim, J. Song, J. P. Baboo, W. Park, D. Ahn, J. Han, L. Gu, Y. Wang, Y.-S. Hu, Y.-K. Sun, J. Kim, *NPG Asia Mater* **2014**, *6*, e138.

[14] E. Uchaker, Y. Z. Zheng, S. Li, S. L. Candelaria, S. Hu, G. Z. Cao, *J. Mater. Chem. A* **2014**, *2*, 18208.

[15] Z. Bi, M. P. Paranthaman, P. A. Menchhofer, R. R. Dehoff, C. A. Bridges, M. Chi, B. Guo, X.-G. Sun, S. Dai, *J. Power Sources* **2013**, *222*, 461.

[16] D. Su, S. Dou, G. Wang, *Chem. Mater*. **2015**, *27*, 6022.

[17] a) M. Sadakane, T. Asanuma, J. Kubo, W. Ueda, *Chemistry of Materials* **2005**, *17*, 3546; b) C. M. Doherty, R. A. Caruso, B. M. Smarsly, C. J. Drummond, *Chem. Mater.* **2009**, *21*, 2895; c) Z. Liang, G. Zheng, W. Li, Z. W. Seh, H. Yao, K. Yan, D. Kong, Y. Cui, *ACS Nano* **2014**, *8*, 5249.

[18] H. Kim, M. G. Kim, J. Cho, *Adv. Energy Mater.* **2012**, *2*, 1425.

[19] J. S. King, E. Graugnard, C. J. Summers, *Adv. Mater*. **2005**, *17*, 1010.

[20] a) M. Zhou, J. Bao, Y. Xu, J. Zhang, J. Xie, M. Guan, C. Wang, L. Wen, Y. Lei, Y. Xie, *ACS Nano* **2014**, *8*, 7088; b) M. Zhou, H. B. Wu, J. Bao, L. Liang, X. W. Lou, Y. Xie, *Angew. Chem. Int. Ed.* **2013**, *52*, 8579; c) H. Zhao, M. Zhou, L. Wen, Y. Lei, *Nano Energy* **2015**, *13*, 790.

[21] W. F. Zhang, Y. L. He, M. S. Zhang, Z. Yin, Q. Chen, *J. Phys. D: Appl. Phys.* **2000**, *33*, 912.

[22] F. D. Hardcastle, H. Ishihara, R. Sharma, A. S. Biris, *J. Mater. Chem.* **2011**, *21*, 6337; A. Felske, W. J. Plieth, *Electrochim. Acta* **1989**, *34*, 75.

[23] B. Erdem, R. A. Hunsicker, G. W. Simmons, E. D. Sudol, V. L. Dimonie, M. S. El-Aasser, *Langmuir* **2001**, *17*, 2664.

[24] D. O. Scanlon, C. W. Dunnill, J. Buckeridge, S. A. Shevlin, A. J. Logsdail, S. M. Woodley, C. R. A. Catlow, M. J. Powell, R. G. Palgrave, I. P. Parkin, G. W. Watson, T. W. Keal, P. Sherwood, A. Walsh, A. A. Sokol, *Nat. Mater. 2013, 12*, 798.

[25] Y. Xu, M. Zhou, L. Wen, C. Wang, H. Zhao, Y. Mi, L. Liang, Q. Fu, M. Wu, Y. Lei, *Chem. Mater.* **2015**.

[26] a) Y. Xu, E. Memarzadeh Lotfabad, H. Wang, B. Farbod, Z. Xu, A. Kohandehghan, D. Mitlin, *Chem. Comm.* **2013**, *49*, 8973; b) K.-T. Kim, G. Ali, K. Y. Chung, C. S. Yoon, H. Yashiro, Y.-K. Sun, J. Lu, K. Amine, S.-T. Myung, *Nano Lett.* **2014**, *14*, 416; c) Wu, D. Buchholz, D. Bresser, L. Gomes Chagas, S. Passerini, *J. Power Sources* **2014**, *251*, 379; d) L. Wu, D. Bresser, D. Buchholz, S. Passerini, *J. Electrochem. Soc.* **2015**, *162*, A3052; e) J. C. Perez-Flores, C. Baehtz, A. Kuhn, F. Garcia-Alvarado, J. Mater. *Chem. A* **2014**, *2*, 1825; f) J. P. Huang, D. D. Yuan, H. Z. Zhang, Y. L. Cao, G. R. Li, H. X. Yang, X. P. Gao, *RSC Adv.* **2013**, *3*, 12593.

[27] S.-M. Oh, J.-Y. Hwang, C. S. Yoon, J. Lu, K. Amine, I. Belharouak, Y.-K. Sun, *ACS Appl. Materials & Interfaces* **2014**, *6*, 11295.

[28] C. Chen, Y. Wen, X. Hu, X. Ji, M. Yan, L. Mai, P. Hu, B. Shan, Y. Huang, *Nat. Comm.* **2015**, *6*.

[29] Y. Zhu, L. Peng, D. Chen, G. Yu, *Nano Lett.* **2016**, *16*, 742.

[30] S. Lunell, A. Stashans, L. Ojamäe, H. Lindström, A. Hagfeldt, *J. Am. Chem. Soc.* **1997**, *119*, 7374.

[31] J. S. Chen, Y. L. Tan, C. M. Li, Y. L. Cheah, D. Luan, S. Madhavi, F. Y. C. Boey, L. A. Archer, X. W. Lou, *J. Am. Chem. Soc.* **2010**, *132*, 6124.

[32] B. Enright, G. Redmond, D. Fitzmaurice, *J. Phys. Chem.* **1994**, *98*, 6195.

[33] T. Xia, W. Zhang, W. Li, N. A. Oyler, G. Liu, X. Chen, *Nano Energy* **2013**, *2*, 826.

[34] T. Zhou, Y. Zheng, H. Gao, S. Min, S. Li, H. K. Liu, Z. Guo, *Adv. Sci.* **2015**, *2*, n/a.

[35] H. Li, X. Huang, L. Chen, *J. Power Sources* **1999**, *81–82*, 340.

[36] M. Zhou, J. Bao, M. Tao, R. Zhu, Y. Zeng, Z. Wei, Y. Xie, *Chem. Comm.* **2012**, *48*, 3439.

[37] A. A. Belak, Y. Wang, A. Van der Ven, *Chem. Mater*. **2012**, *24*, 2894.

[38] K. Shen, *Ph.D Thesis*, Delft University of Technology, September, **2014**

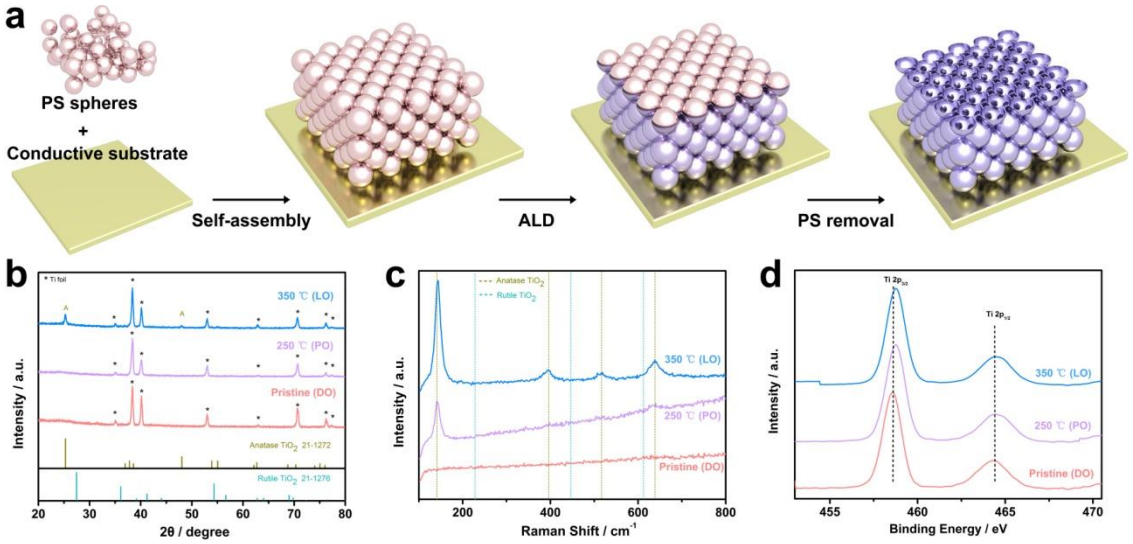

Figure 1. (a) Schematic illustration of the fabrication processes. Half of the top layer is peeled off in the scheme to illuminate the inner details; (b,c,d) Temperature dependence of XRD patterns (b), Raman spectra (c) and XPS spectra (d).

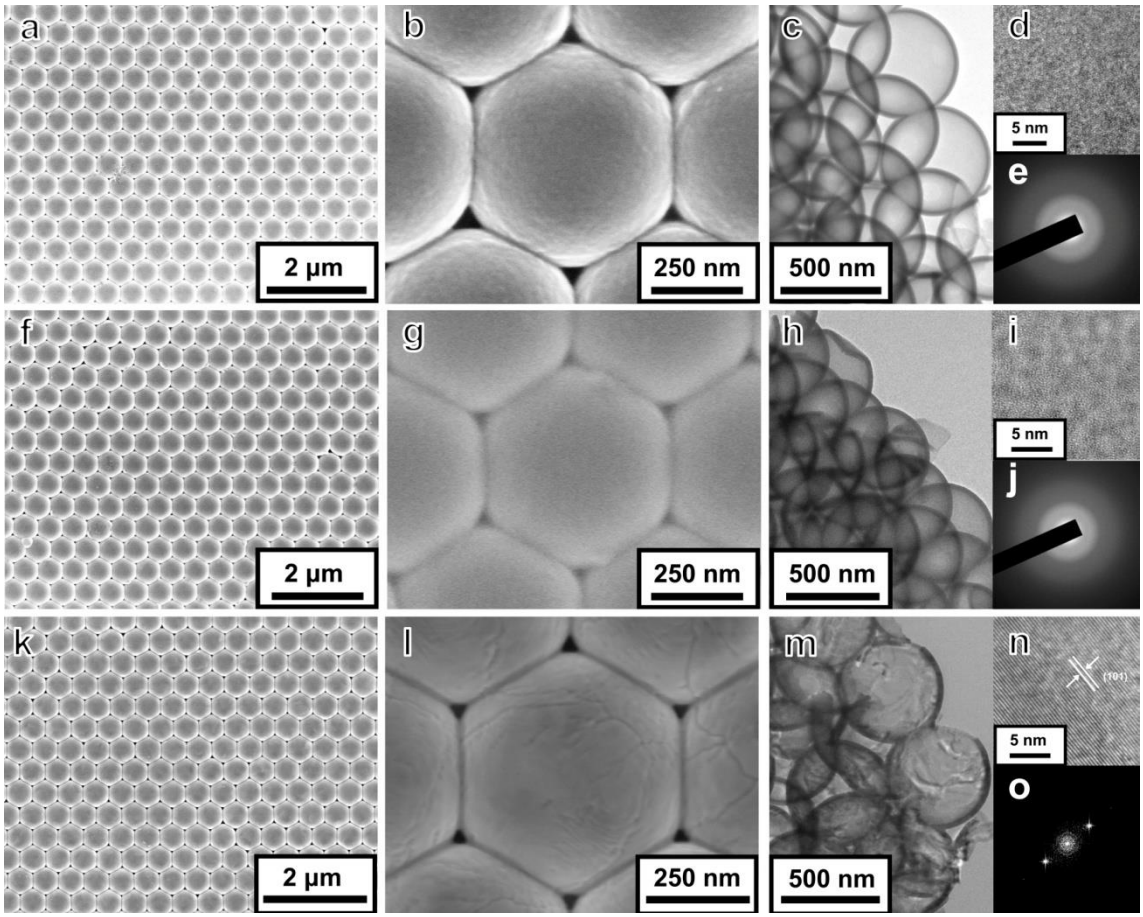

Figure 2. Morphology characterizations of disordered (DO, a-e), partially ordered (PO, f-j) and long-rang ordered (LO, f-j) TiO_2 architectures. (a, b, f, g, k, i) Typical top-view SEM images corresponding inverse opal architecture at low and high magnifications; (c, d, h, i, m, n) Typical TEM and HRTEM images in edge part; (e, j) Typical SAED pattern of (c, h); (o) fast Fourier transform (FFT) image based on the lattice fringe in (n).

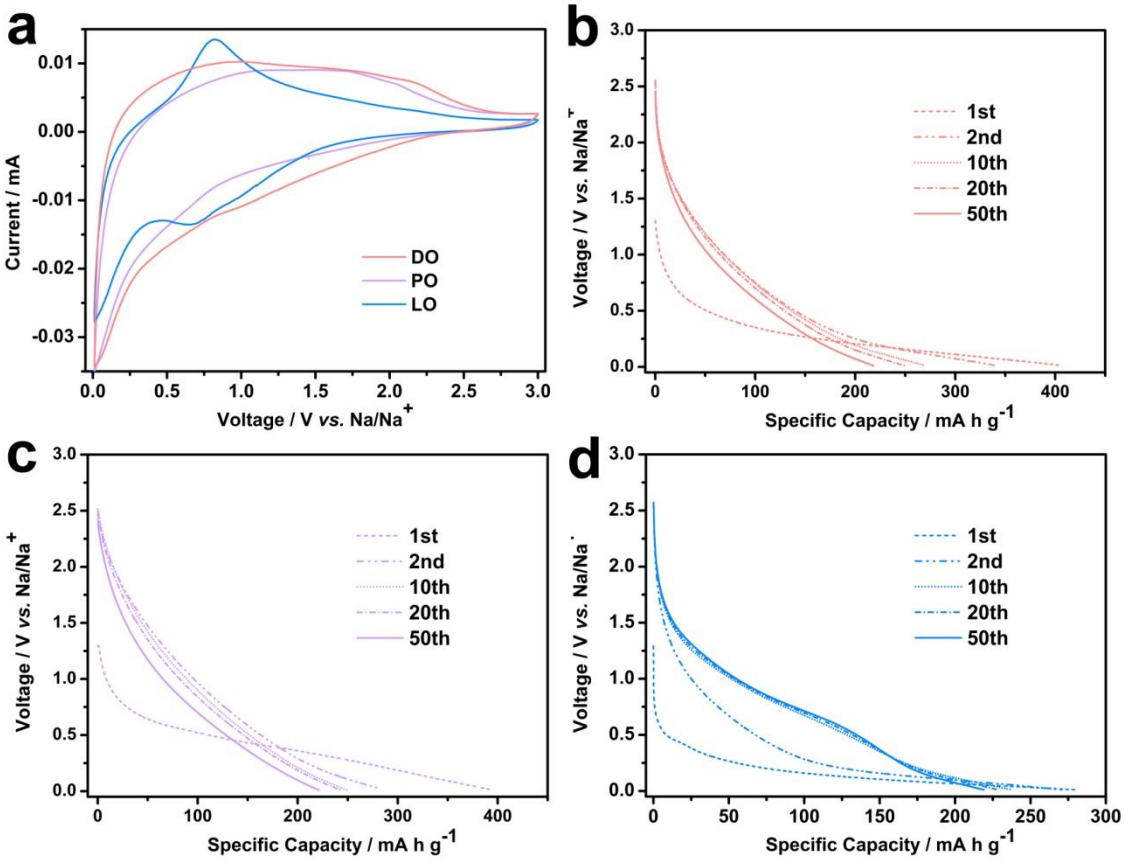

Figure 3. The CV curves at a scan rate of 0.1 mV s^{-1} in the potential range of 0.01-3.0 V of TiO_2 electrodes with different atomic ordering. (b, c, d) Sodiation voltage profiles at 50 mA g^{-1} of DO (b), PO (c) and LO (d).

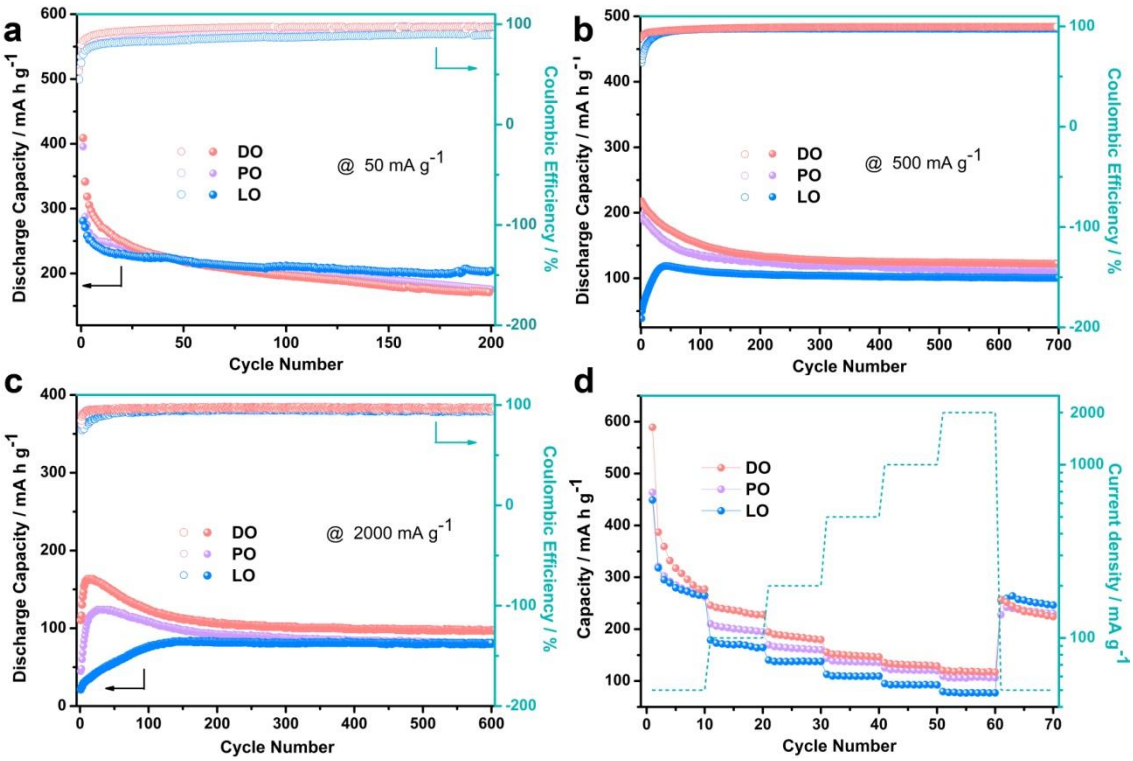

Figure 4. (a-c) Cycling performance of DO, PO and LO at different charging/discharging current density: (a) 50 mA g^{-1}; (b) 500 mA g^{-1}, (c) 2000 mA g^{-1}; (d) Rate capability of DO, PO and LO.

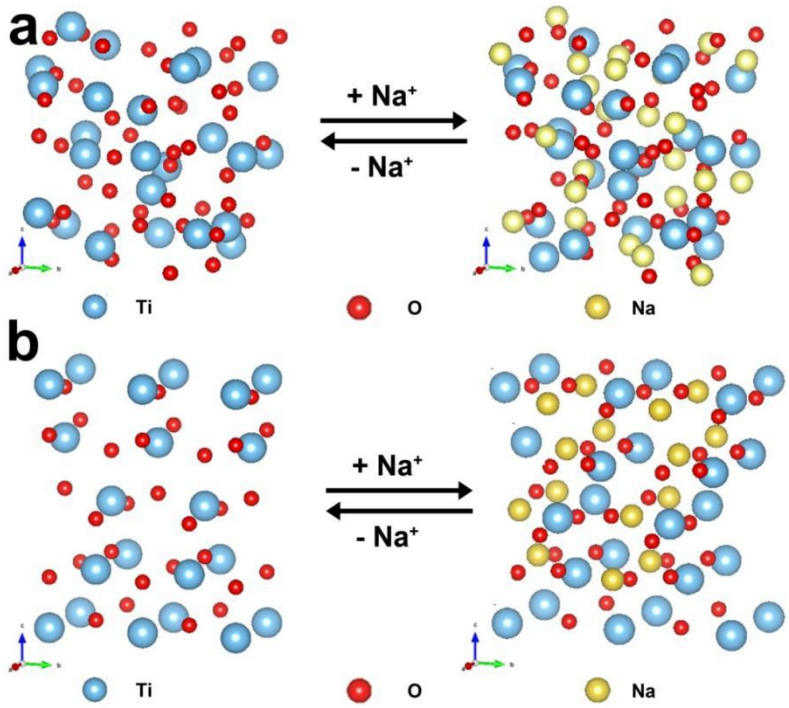

Figure 5. Schematic simulation of atomic arrangement of disordered (a) and long-range ordered TiO_2 (anatase) (b) before and after Na-ion insertion.

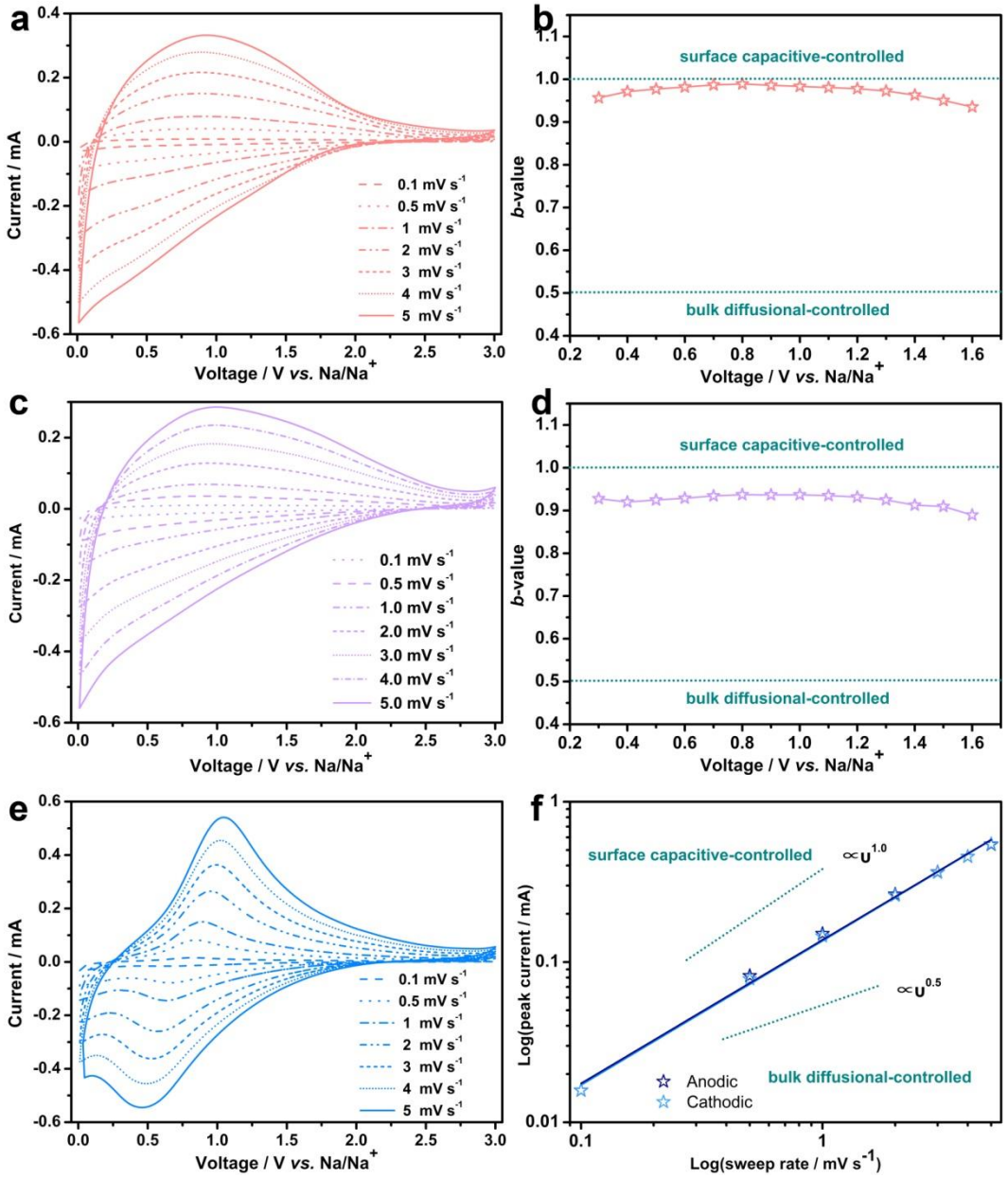

Figure 6. Kinetics analysis of the electrochemical behaviors toward Na ions. (a, c, e) CV curves at various sweep rates from 0.1 to 5 mV s^{-1} of DO (a), PO (c) and LO (e); (b, d) *b*-values for DO and PO as a function of potential for anodic sweep; (d) Determination of *b*-values for LO based on the anodic and cathodic current at peak potential.

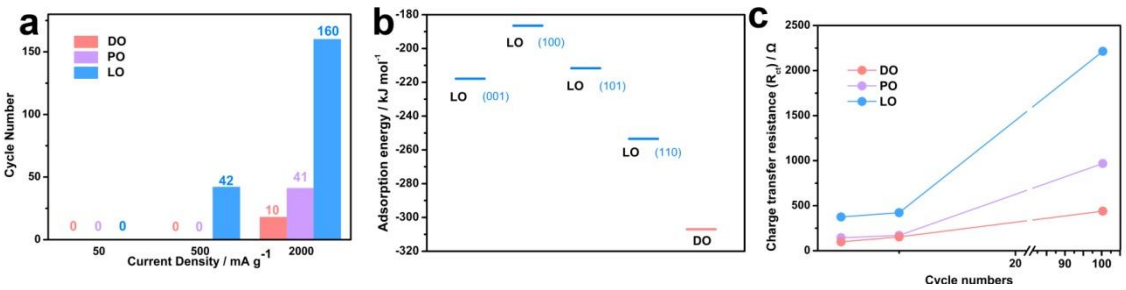

Figure 7. Analysis of surface orderliness: (a) The performance comparison among DO, PO and LO of self-improving process; (b) Absorption energy of Na ions in propylene carbonate (PC); (c) Charge transfer resistence (R_{ct}) after different cycles.

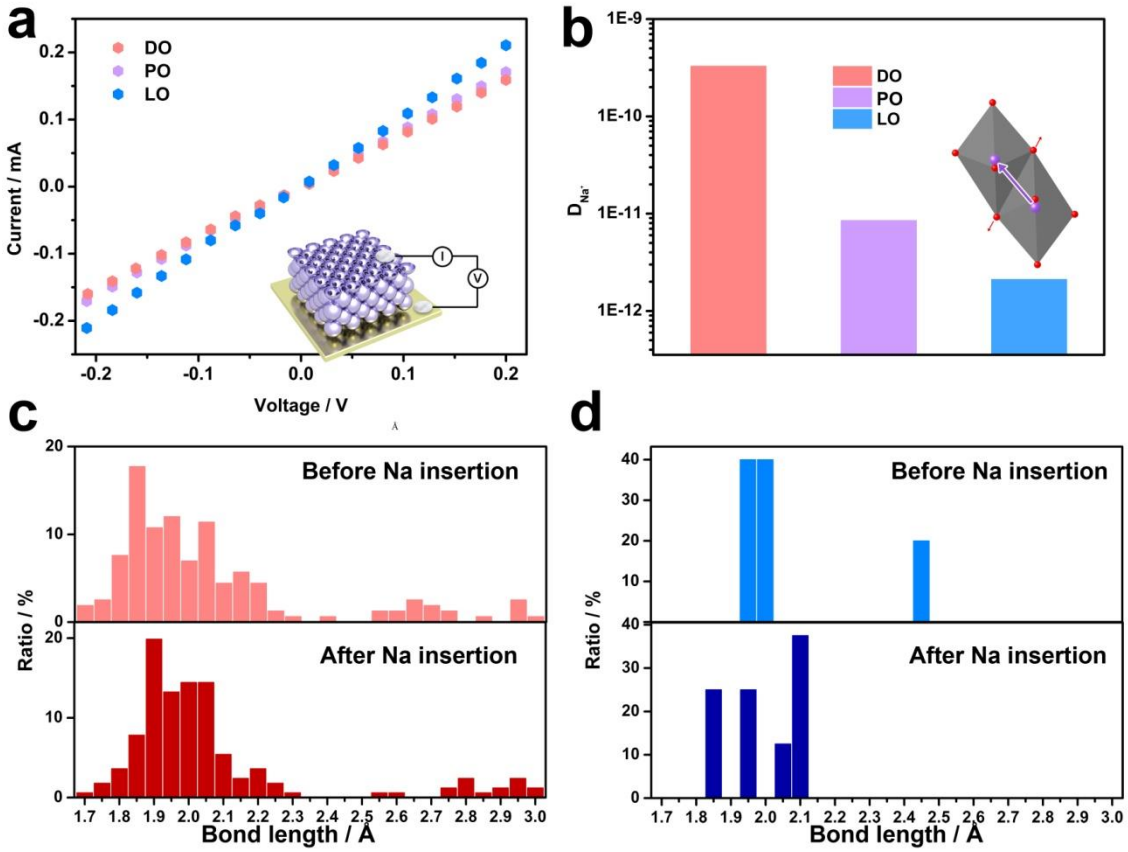

Figure 8. Analysis of bulk orderliness: (a) Resistance from Current−voltage (I−V) characteristics. Shown in inset of (a) is the schematic view of the testing devices; (b) ion diffusion coefficient (D_{Na}^{+}). Inset: the schematic varying of the Na-O_6 octahedra during the (de-)sodiation. Red: O atoms. Violet: Na atoms. The arrays show the directions of Na-ion hopping and expansion of octahedrons. (c) The distribution of bond length of Ti-O before and after Na insertion in DO, (d) The distribution of bond length of Ti-O before and after Na insertion in LO.